Squared-like BiOCl nanosheets synthesized by ethylene glycol-assisted solvothermal method and their photocatalytic performance*

HU Jia-jia (胡家佳), **LIU Jia-qin** (刘家琴), **RUAN Li-li** (阮丽丽), **BIAN Hai-dong** (卞海东), **ZHANG Xin-yi** (张信义), **and WU Yu-cheng** (吴玉程)**

Laboratory of Functional Nanomaterials and Devices, School of Materials Science and Engineering, Hefei University of Technology, Hefei 230009, China

(Received 25 September 2014)

Bismuth oxychloride (BiOCl) with morphology of squared-like nanosheet is synthesized by solvothermal method using ethylene glycol aqueous reaction solution. The product is characterized by X-ray powder diffraction (XRD), scanning electron microscopy (SEM), energy dispersive spectroscopy (EDS), transmission electron microscopy (TEM) and ultraviolet-visible (UV-Vis) diffuse reflection spectroscopy, respectively. The layered structure, the hydrogen bonding between hydroxyl groups and their selective adsorption cause the formation of the squared-like nanosheets. The photocatalytic degradation activity of the as-prepared BiOCl is tested by the degradation of methyl orange under UV light irradiation. Repeating the degradation process four times under the same condition, the results show that the squared-like BiOCl nanosheets present high photocatalytic activity and stability.

Document code: A **Article ID:** 1673-1905(2015)01-0005-5

DOI 10.1007/s11801-015-4170-7

In the past two decades, semiconductor photocatalysts have attracted considerable attention for the treatment of organic contaminants in waste water[1,2]. Bismuth oxychloride (BiOCl) is talent showing itself owing to its high catalytic activity and chemical stability among a large number of photocatalysts[3]. Although BiOCl is a wide band gap semiconductor with a band gap of about 3.4 eV[4], it can effectively photodegrade organic pollutants because of the unique layer structure. PbFCl-type BiOCl belongs to tetragonal system[5] with the layer structure expressed as [Cl-Bi-O-Bi-Cl][6]. The layer-structured BiOCl has enough space to polarize the corresponding atoms and atomic orbit, and the induced dipole moment could effectively separate the photo-induced electrons and holes[7]. Moreover, BiOCl is a kind of indirect semiconductor[8] which is efficient to decrease the recombination rate of photo-induced electrons and holes.

Recently, BiOCl has been widely studied because of its excellent optical properties and promising industrial applications. For instance, Zhang et al[9] synthesized BiOCl single-crystalline nanosheets with selectively exposed {001} and {010} facets using a facile hydrothermal route. It was found that the BiOCl with exposing different facets exhibited different photocatalytic activities. Chen et al[10] synthesized BiOCl microspheres composed of numerous nanoplates via a hydrothermal route, and found that the obtained BiOCl exhibited high photocatalytic activities for the degradation of RhB, MO and phenol. Yu et al[11] synthesized BiOCl with tunable morphologies from nanoflakes to hollow microspheres (HMSs) by hydrothermal process, and the as-prepared BiOCl exhibited much higher photocatalytic activity than the common one. In this paper, BiOCl nanosheets are prepared by a different hydrothermal method.

Bismuth nitrate pentahydrate ($Bi(NO_3)_3·5H_2O$), sodium chloride (NaCl) and ethylene glycol (EG) were purchased from Sinopharm Chemical Reagent Co., Ltd. (Shanghai, China). All reagents were analytical grade, and were used as received without further purification.

In a typical process, 2.425 g $Bi(NO_3)_3·5H_2O$ (5 mmol) was dissolved in 25 mL EG, and it was recorded as solution A. 0.375 g NaCl was dissolved in 25 mL distilled water, and it was recorded as solution B. Then the solution B was dropwise added into the solution A under stirring, and transferred into a Teflon-lined stainless autoclave. The solvothermal synthesis was conducted at 150 °C for 10 h in an electric oven. The resulting precipitate was washed with ethanol and deionized water for several times. Finally, the white powdered BiOCl was obtained by drying the precipitate at room temperature in air. In comparison, BiOCl microspheres were also prepared by hydrothermal method. The preparation of the BiOCl mi-

* This work has been supported by the National Natural Science Foundation of China (Nos.51272063 and 51172059), and the Natural Science Foundation of Anhui Province (No.1408085QE85).

** E-mail: ycwu@hfut.edu.cn

crospheres was a little different from that of BiOCl nanosheets, where the solution B was 25 mL EG dissolving 0.375 g NaCl, and the solvothermal procedure was conducted at 150 °C for 5 h, the other steps were the same as the preparation of BiOCl nanosheets.

X-ray diffraction (XRD) patterns, performed on a D/MAX2500V using Cu Kα radiation at a 2θ scan rate of 2°/min from 5° to 70°, were used to confirm the phase identity and the size of crystalline grains. The morphology and the microstructures of the products were investigated by field emission scanning electron microscope (FESEM, FEI Sirion 200 and Hitachi SU8020) and high resolution transmission electron microscope (HRTEM, JEM-2100F), respectively. The ultraviolet-visible (UV-Vis) diffuse reflectance spectroscopy (DRS) measurement was carried out at room temperature on a UV3600 spectrometer (Shimadzu, Japan) by using $BaSO_4$ as the reference.

Methyl orange (MO) solution was used to evaluate the photocatalytic activity of BiOCl powder. 0.02 g photocatalyst powders were placed in 15 mL 20 mg/L MO solution with vigorous stirring for 30 min to achieve the adsorption/desorption equilibrium in the dark. A 300 W high-pressure mercury lamp with a maximum emission wavelength of 364 nm was used as UV light irradiation. The photocatalytic reactions were performed on an XPA-7 photochemical reactor (Nanjing Xujiang Machine-electronic Company, China). The distance between the solution and the lamp was kept at 10 cm. A UV1800 spectrometer (Shimadzu, Japan) was used to record the concentration of MO during light irradiation.

Fig.1 shows the XRD patterns of the as-synthesized samples of BiOCl nanosheets and BiOCl microspheres. All the diffraction peaks in the both two XRD patterns are perfectly in good agreement with the tetragonal phase of BiOCl (JCPDS No.06-0249). Moreover, the intense and sharp diffraction peaks indicate that the products are well-crystallized, and the intensity of diffraction peaks of BiOCl nanosheets is higher than that of BiOCl microsphere. The most intense diffraction peak of BiOCl nanosheets corresponds to the (001) plane, while the highest peak of BiOCl microspheres corresponds to the (110) plane.

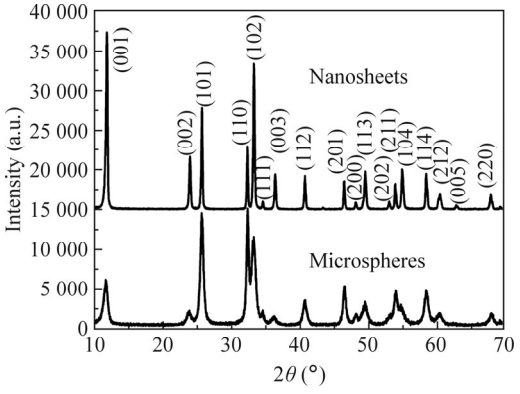

Fig.1 XRD patterns of the as-synthesized BiOCl nanosheets and BiOCl microspheres

As shown in Fig.2(a) and (b), the BiOCl sample is composed of a large number of well-defined and uniform squared-like nanosheets with width of 300–600 nm and thickness of 30–60 nm. The BiOCl nanosheets with the width of 600 nm are well defined and selectively exposed facets. The BiOCl microspheres with an average diameter of 1–3 μm are uniformly dispersed without aggregation. As the high-magnification SEM image of BiOCl microspheres shown in Fig.2(d), the surfaces of the microspheres are surrounded by a lot of irregular nanosheets. According to the energy dispersive spectroscopy (EDS) shown in Fig.2(e) and (f), there are only Bi, O, Cl and Si elements in the EDS spectra of BiOCl samples, where silicon slice is used as observation carrier, and the result confirms that the ratios of Bi:O for BiOCl nanosheets and BiOCl microspheres are 5.3:4.6 and 26.1:22.3 (atomic ratio), respectively, which are both consistent with the theoretical value of 1:1.

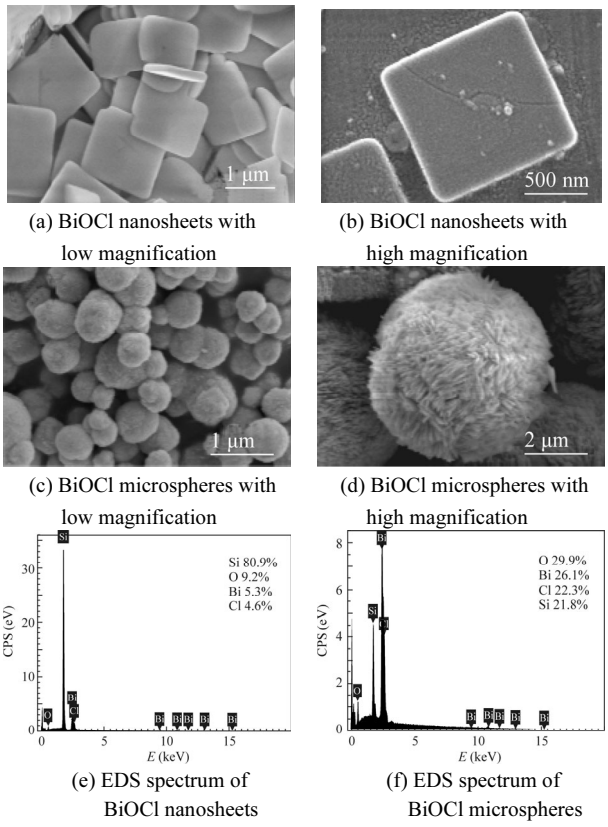

(a) BiOCl nanosheets with low magnification
(b) BiOCl nanosheets with high magnification
(c) BiOCl microspheres with low magnification
(d) BiOCl microspheres with high magnification
(e) EDS spectrum of BiOCl nanosheets
(f) EDS spectrum of BiOCl microspheres

Fig.2 SEM images and EDS spectra of BiOCl samples

The transmission electron microscope (TEM) image of the as-synthesized squared-like BiOCl is shown in Fig.3(a). It is clearly observed that the width of the well-defined squared-like BiOCl nanosheet is approximately 600 nm, which is in good agreement with the result discussed above. Fig.3(b) shows the HRTEM image of a single BiOCl nanosheet, which demonstrates the clear lattice fringes and further confirms the single crystal structure of the BiOCl nanosheets. The interplanar spacing is 0.278 nm corresponding to the (110) planes of the tetragonal system of BiOCl. The inset of Fig.3(b) shows the selected area electron diffraction (SAED) pattern of

the single BiOCl nanosheet, and it can be seen that the angle labeled is 45°, which is in agreement with the theoretical value of the angle between (110) and (200) planes. The set of diffraction spots can be indexed as the [001] zone axis of tetragonal BiOCl. The SAED pattern and HRTEM image indicate that the growth direction of these BiOCl nanosheets is along the c axis, which well agrees with the XRD result discussed above.

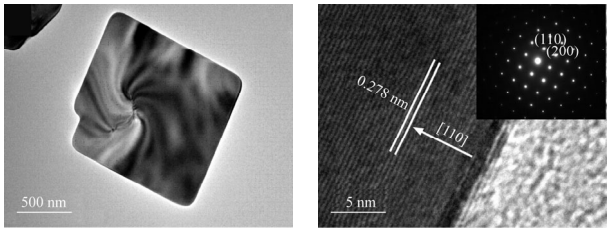

(a) (b)

Fig.3 (a) TEM image, (b) HRTEM image and SAED pattern (inset) of the as synthesized squared-like BiOCl nanosheets

The experiments with different reaction times were conducted to study the formation process of the squared-like BiOCl nanosheets. It is observed that all the diffraction peaks in the XRD patterns are completely in good agreement with the tetragonal phase of BiOCl (JCPDS No.06-0249). The diffraction peaks of BiOCl sample without hydrothermal treatment are broader and weaker compared with those of the samples after hydrothermal process, which indicates that the hydrothermal treatment of the samples greatly improves the crystallinity. The diffraction peaks become sharper and stronger with the increase of reaction time, which demonstrates that the crystallinity is improved as the increase of hydrothermal reaction time. When the hydrothermal reaction time reaches 10 h, the diffraction peak intensity of the (001) plane is much stronger than those of other planes, suggesting that the exposed planes of BiOCl nanosheets are mainly (001) planes.

Before hydrothermal process, the morphology of BiOCl shown in Fig.4(f) is flower-like structure assembled with nanoparticles. However, the flower-like structure is completely destroyed and transformed into tiny nanoplates even after the hydrothermal treatment only for 2 h. With the increase of hydrothermal reaction time, the nanoplates gradually become larger and regular under the Ostwald ripening effect. After the hydrothermal process for 10 h, the BiOCl is completely transformed into regular squared-like nanosheets.

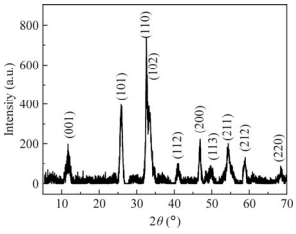

(a) XRD before treatment

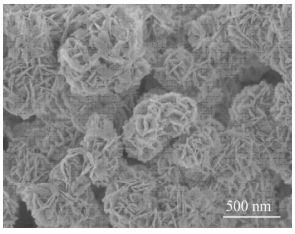

(f) SEM before treatment

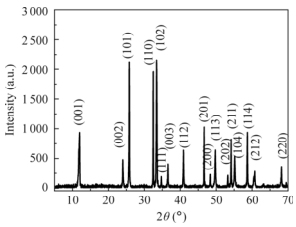

(b) XRD after 2 h

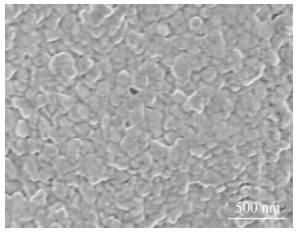

(g) SEM after 2 h

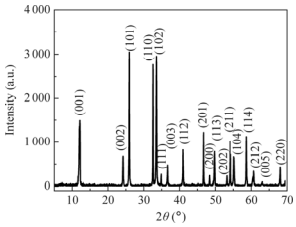

(c) XRD after 4 h

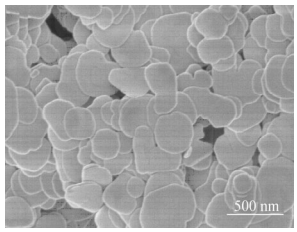

(h) SEM after 4 h

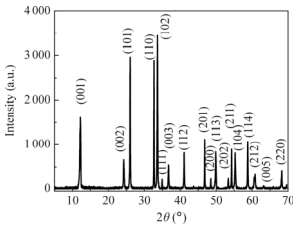

(d) XRD after 6 h

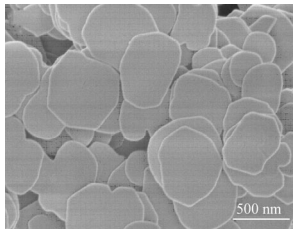

(i) SEM after 6 h

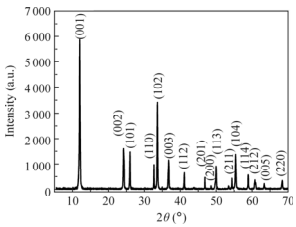

(e) XRD after 10 h

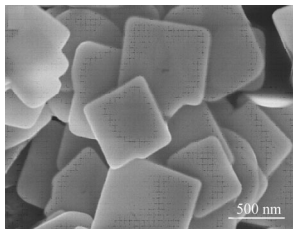

(j) SEM after 10 h

Fig.4 (a)–(e) XRD patterns and (f)–(j) SEM images of BiOCl samples after different hydrothermal reaction times

To explore the function of the solvents in the formation of squared-like BiOCl nanosheets, the experiments with different water and EG solvents were conducted, respectively. As shown in Fig.5(c), the BiOCl synthesized in pure EG solvent has the morphology of microspheres as discussed above. However, when distilled water solvent is used, as shown in Fig.5(b), the sample can be indexed to tetragonal BiOCl phase (JCPDS No.06-0249). Furthermore, the SEM image shows that the main morphology of the BiOCl sample synthesized in pure distilled water solvent is composed of a large number of irregular and nonuniform nanosheets.

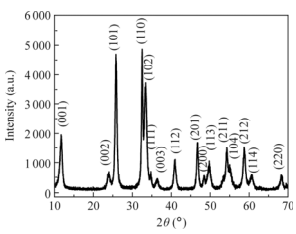

(a) XRD in EG

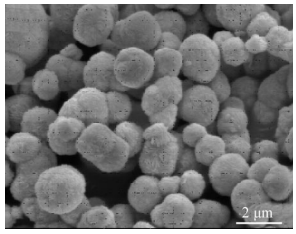

(c) SEM in EG

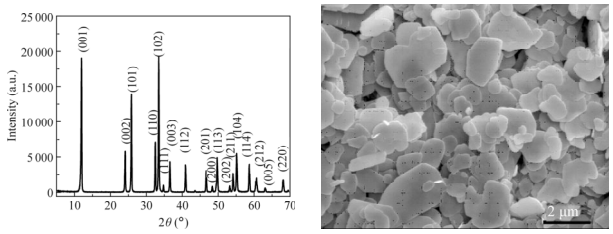

(b) XRD in water (d) SEM in water

Fig.5 XRD patterns and SEM images of BiOCl samples synthesized in pure EG solvent and pure water solvent

EG has some special chemical and physical properties, such as basicity, chelation, vapor pressure and viscosity[12], which are expected to direct the crystal growth of BiOCl. Because of the effects of hydrogen bonding between hydroxyl groups, EG molecules can exist in long chains which serve as soft template, inducing the formation of sphere-like superstructures. This is the reason why the shape of resulted sample is microsphere when the solvent is pure EG.

In the preparation of squared-like BiOCl nanosheets, the distilled water replaces some of EG as the reaction solvent. Because of the presence of water, some effects of EG are weakened, such as viscosity and chelation, which prohibits the formation of sphere-like superstructures but leads to a plate-growth along the [001] direction due to the layered structure of bismuth oxyhalides.

Based on the above results and analysis, the formation process of squared-like BiOCl nanosheets can be summarized as follows. BiOCl has a layered structure characterized by $[Bi_2O_2]$ slabs interleaved by double slabs of Cl atoms, which results in the general formation of plate morphology. So as long as the BiOCl nanoparticles form in the early stage, they tend to grow into nanoplates[13]. With the start of solvothermal process, these tiny nanosheets grow rapidly along the [001] direction, and finally completely transform into nanosheets, when the reaction time is increased to 10 h because of the hydrogen bonding between hydroxyl groups and its selective adsorption.

Fig.6(a) shows the UV-Vis diffuse reflectance spectra of the two kinds of BiOCl photocatalysts. The absorbance limits of the two kinds of BiOCl are both less than 400 nm, which indicates that the BiOCl photocatalysts only have response to UV light. The band gap of a semiconductor is determined by $\alpha h\upsilon = A(h\upsilon - E_g)^{n/2}$, where α, υ, A and E_g are the absorption coefficient, light frequency, proportionality constant and band gap energy, respectively[14,15]. Among them, n depends on the characteristics of the transition in a semiconductor, i.e., n=1 for direct transition or n=4 for indirect transition. Here, n is 4 because BiOCl is an indirect semiconductor[16]. Therefore, the band gap energies of the BiOCl samples can be estimated from $(\alpha h\upsilon)^{1/2}$ versus the photon energy ($h\upsilon$) as shown in Fig.6(b). The intercept of the tangent to the x-axis can give a good approximation of the band gap energies for the BiOCl nanosheets. The estimated band gap energy of the BiOCl nanosheets is about 3.48 eV, which is almost the same as the theoretic value of 3.46 eV, while that of BiOCl microspheres is about 3.25 eV, which is lower than the reported value.

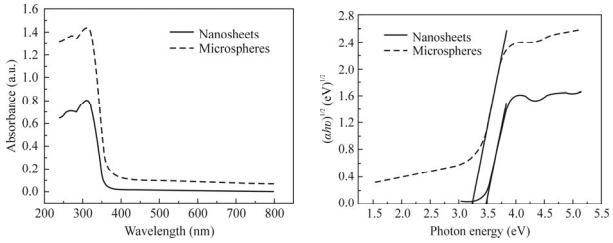

(a) (b)

Fig.6 (a) UV-Vis diffuse reflectance spectra of the as-synthesized BiOCl powders; (b) $(\alpha h\upsilon)^{1/2}$ versus the photon energy ($h\upsilon$) for the BiOCl powders

Before irradiation, the adsorption/desorption equilibrium is obtained by stirring vigorously for 30 min in dark. Fig.7(a) shows the absorption spectra of MO solution degraded by squared-like BiOCl nanosheets with different irradiation times. The characteristic absorption peak of MO at 464 nm is used to detect the photocatalytic degradation process. The MO adsorption rate is about 5% after 30 min adsorption/desorption. The absorption peak at 464 nm decreases gradually with the increase of irradiation time, and disappears completely within 15 min. Fig.7(b) shows the absorption spectra of MO solution degraded by BiOCl microspheres with different irradiation times. The adsorption rate is about 25% when the adsorption/desorption equilibrium is achieved, which is much higher than that of BiOCl nanosheets (5%). Then the absorption intensity peak of MO solution gradually decreases with the increase of irradiation time, and the degradation rate reaches 50% after 15 min irradiation. Fig.7(c) shows the ratio of MO concentration C to initial MO concentration C_0 versus the irradiation time. In Fig.7(c)–(e), the data of 0 min are the values after achieving the adsorption/desorption equilibrium. MO concentration decreases gradually as the increase of degradation time under UV light. After irradiating for 15 min, the degradation rates of BiOCl nanosheets and microspheres are 100% and 56%, respectively, indicating that the photocatalytic activity of BiOCl nanosheets is much higher than that of BiOCl microspheres under UV light irradiation.

To evaluate the stability of BiOCl samples in the photocatalytic reaction, BiOCl nanosheets and BiOCl microspheres are reclaimed and re-examined for three extra cycles under the same condition. As shown in Fig.7(d), after 4 times of photodegradation of MO, the photocatalytic activity of BiOCl nanosheets is decreased to 85%. Also, the photocatalytic activity of BiOCl microspheres is decreased from 50% to less than 20% accompanied with the decrease of adsorption ability from 25% to 9% during continuous reusing process. The photocatalytic performance of BiOCl samples after a month is measured, and the degradation rates are shown in Fig.7(e). The degradation rates of BiOCl nanosheets

and BiOCl microspheres are 84% and 55%, respectively, and the values are both decreased. The results indicate that BiOCl nanosheets have better photocatalytic performance and higher stability on the degradation of MO compared with BiOCl microspheres.

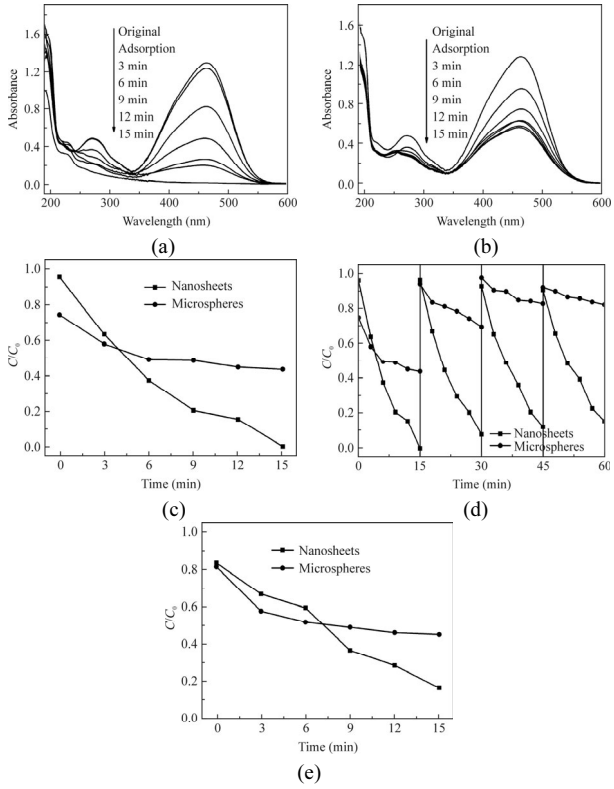

Fig.7 Absorption spectra of MO solution degraded by (a) BiOCl nanosheets and (b) BiOCl microspheres with different irradiation times; (c) The variations of MO concentration (C/C_0) with irradiation time over different photocatalysts; (d) Recycling experiment results of degrading MO under UV-vis irradiation; (e) The variations of MO concentration (C/C_0) with irradiation time over different photocatalysts after a month

BiOCl has a layered structure formed by alternately arranging double Cl atoms layers and $[Bi_2O_2]$ layers along the c-axis, which can induce the internal static electric fields perpendicular to the $[Bi_2O_2]$ slabs and Cl slabs, separate the photo-induced electrons and holes effectively, and result in high photocatalytic performance. Through the XRD patterns, SAED patterns and HRTEM images, we can find that the most exposed facets of BiOCl nanosheets are the (001) facets, which is the reason why BiOCl nanosheets have high photocatalytic activity under UV light irradiation. The porous structure makes the adsorption ability of BiOCl microspheres much higher than that of BiOCl nanosheets. However, the porous structure and strong adsorption block the release of photocatalytic reaction products from the surface of BiOCl microspheres, and obstruct the contact between MO molecules and catalyst. On the contrary, the smooth surface and excellent dispersibility produce the convenient adsorption of MO and the release of reaction products, which can enhance the photocatalytic activity greatly.

In summary, BiOCl with morphology of nanosheets was synthesized by solvothermal method using EG aqueous solution. The XRD, SEM, SAED and HRTEM characterizations show that the powders are squared-like BiOCl nanosheets with exposed (001) facets, which results in the improved photocatalytic performance under UV light irradiation. The degradation of MO solution proves that BiOCl nanosheets have a good photocatalytic activity in contrast to the BiOCl microspheres under UV light. Recycling experiments also confirm the long term stability of the BiOCl nanosheets as photocatalyst under UV light irradiation.

References

[1] S. D. Sharma, K. K. Saini, C. Kant, C. P. Sharma and S. C. Jain, Applied Catalysis B: Environmental **84**, 233 (2008).

[2] X. C. Ni, L. X. Sang, H. J. Zhang, K.-K. Anoop, A. Salvatore, X. Wang, F. Rosalba, T. Li, M. L. Hu and L. J. Xu, Optoelectronics Letters **10**, 43 (2014).

[3] Y. Lei, G. Wang, S. Song, W. Fan and H. Zhang, Cryst. Eng. Comm. **11**, 1857 (2009).

[4] H. Peng, C. K. Chan, S. Meister, X. F. Zhang and Y. Cui, Chemistry Materials **21**, 247 (2009).

[5] L. S. Zhang, W. Z. Wang, Z. G. Chen, L. Zhou, H. L. Xu and W. Zhu, Journal of Materials Chemistry **17**, 2526 (2007).

[6] C. F. Guo, S. Cao, J. Zhang, H. Tang, S. Guo, Y. Tian and Q. Liu, Journal of American Chemical Society **133**, 8211 (2011).

[7] X. Lin, T. Huang, F. Huang, W. Wang and J. Shi, J. Phys. Chem. B **110**, 24629 (2006).

[8] K.-L. Zhang, C.-M. Liu, F.-Q. Huang, C. Zheng and W.-D Wang, Applied Catalysis B: Environmental **68**, 125 (2006).

[9] J. Jiang, K. Zhao, X. Y. Xiao and L. Z. Zhang, Journal of American Chemical Society **134**, 4473 (2012).

[10] F. Chen, H. Q. Liu, S. Bagwasi, X. X. Shen and J. L. Zhang, Journal of Photochemistry and Photobiology A: Chemistry **215**, 76 (2010).

[11] K. Zhang, J. Liang, S. Wang. J. Liu, K. X. Ren, X. Zheng, H. Luo, Y. J. Peng, X. Zou, X. Bo, J. H. Li and X. B. Yu, Crystal Growth & Design **12**, 793 (2012).

[12] M. Shang, W. Wang and H. Xu, Crystal Growth & Design **9**, 991 (2009).

[13] D. Q. Zhang, M. C. Wen, B. Jiang, G. S. Li and Jimmy C. Yu, Journal of Hazardous Materials **211-212**, 104 (2012).

[14] J. Henle, P. Simon, A. Frenzel, S. Scholz and S. Kaskel, Chemistry of Materials **19**, 366 (2007).

[15] J. Z. Huang, S. Y. Liu, N. N. Yao and X. J. Xu, Optoelectronics Letters **10**, 161 (2014).

[16] E. J. Li, K. Xia, S. F. Yin, W. L. Dai, S. L. Luo and C. T. Au, Materials Chemistry and Physics **125**, 236 (2010).